Global Survey of the MJO and Extreme Precipitation

Enter authors here: Carl J. Schreck III[1]

[1]Cooperative Institute for Satellite Earth System Studies (CISESS), North Carolina Institute for Climate Studies (NCICS), North Carolina State University (NCSU).

Corresponding author: Carl Schreck (carl_schreck@ncsu.edu)

Key Points:

- The Madden–Julian Oscillation significantly affects extreme precipitation events around the globe and during all seasons.
- Teleconnections with the Madden–Julian Oscillation create strong modulations of extreme precipitation outside the tropics.
- These results could be leveraged for valuable subseasonal forecasts of extreme events to farmers and water resource managers.

Abstract

The Madden–Julian Oscillation (MJO) modulates extreme precipitation events around the globe. Past studies have examined these events for specific regions, but this study leverages global 0.1°-resolution satellite-based precipitation estimates to perform a survey of these modulations at an unprecedented scale. The MJO is generally considered to be a tropical convective phenomenon, and many of the extreme events are tied to that convective core, particularly over Indonesia and South America. However, this study reaffirms the MJO's reach well beyond the tropics through teleconnections. It is particularly influential in modulating extreme events over North America, northern Africa, and Southwest Asia. Given the increasing skill of numerical models for predicting the MJO, these results could lay the groundwork for subseasonal forecasts of extreme events.

Plain Language Summary

The Madden–Julian Oscillation (MJO) is the largest driver of week-to-week changes in tropical weather. It increases the rainfall over the Indian Ocean and then moves eastward. It circles the global tropics over the course of 4–8 weeks. This study shows how the MJO affects heavy rainfall events everywhere. It uses a new satellite-based dataset that estimates daily rainfall every ~10 km. Not surprisingly, the MJO affects extreme rainfall events in its tropical core. It can also lead to extreme events outside of the tropics, likely by changing wind patterns. Some of the most interesting effects happen over North America, northern Africa, and Southwest Asia. State-of-the-art models can predict the MJO's movements 2–3 weeks in advance. A forecaster could use those predictions to anticipate extreme events based on the results of this study. Such a forecast might give farmers and water resource managers the time they need to prepare for those events.

1 Introduction

The Madden–Julian Oscillation (MJO) is the dominant mode of subseasonal tropical variability (Zhang, 2005; Zhang et al., 2013). Because of its intense modulation of tropical convection, it affects weather patterns and extreme events around the globe (Zhang, 2013). These effects include heat waves, cold waves, tropical cyclones, fires, and extreme rainfall events. The MJO lies at the subseasonal interface between weather and climate, so these effects can be critical for long-range forecasts. This study will focus on the MJO's modulation of extreme rainfall in particular.

Numerous studies have examined the MJO's effects on precipitation extremes, but most of these have been regional in scale. For example, flooding events in Sumatra, which lies at the heart of the MJO's convective variability, tend to initiate when the MJO was over the Indian Ocean (phases 2-3) (Baranowski et al., 2020). The MJO's winds also interact strongly with the large topography and moisture availability over South America. When the MJO's convection is over the Central Pacific and Western Hemisphere (phases 8-1), an enhanced South Atlantic Convergence Zone (SACZ) can lead to extreme rainfall over northeastern Brazil (Carvalho et al., 2004; Grimm, 2019; Hirata & Grimm, 2016; Shimizu et al., 2017).

The MJO's teleconnections also affect extreme precipitation outside of the tropics. For example, extreme precipitation events in the United States are significantly more likely when the MJO is active (particularly over the Indian Ocean) than when it is not (Jones & Carvalho, 2012). The MJO modulates drivers for extreme rainfall like atmospheric rivers (Baggett et al., 2017; Mundhenk et al., 2018; Ralph et al., 2011) and tropical cyclones (Klotzbach, 2010; Kossin et al., 2010; Mo, 2000). When The MJO is over the Western Hemisphere (phases 8-1), it also significantly enhances extreme precipitation over arid Southwest Asia (Barlow et al., 2005; Hoell et al., 2018; Nazemosadat et al., 2021; Nazemosadat & Shahgholian, 2017).

Despite these regional studies, fewer have examined the global modulation of precipitation extremes by the MJO. Jones et al. (2004) examined the MJO's effect on 5-day extreme events during November–April. The regions where these extremes occurred broadly followed the MJO's convective envelope and included many of the regional examples above. Aggregated globally, they found that extreme events occurred 40% more often when the MJO was active than when it was not. Jones et al. also demonstrated the ability of a general circulation model (GCM) to replicate these broad patterns.

The current study builds upon Jones et al. (2004) in several key ways. Whereas they only examined November–April when the MJO is most active, this study will explore all seasons. They also used Global Precipitation Climatology Project (GPCP) data, which are 5-day means on a coarse 2.5° grid. This study will leverage the new NASA IMERG dataset, which is a daily 0.1° grid. This fine resolution allows us to exclude precipitation over the oceans where it is less societally relevant. Finally, Jones et al. defined extreme events as the 75th percentile of raining pentads to insure a large sample size. Here, they will be defined as the 2-year event, which are much more extreme (>99th percentile) and more likely to have societal impacts (Leopold, 1968). Numerical models can now skillfully forecast the MJO out to three weeks (Kim et al., 2014; Vitart & Molteni, 2010), so the results of this study may have significant value for subseasonal prediction of extreme rainfall.

2 Data

Precipitation estimates are obtained from the daily NASA IMERG (Integrated Multi-satellitE Retrievals for GPM) dataset (Huffman et al., 2015, 2019). These data are available on a global 0.1° latitude–longitude grid for 1 June 2000–30 June 2020. Only data over land 60°S–60°N are used here. Satellite-based precipitation datasets like IMERG notoriously underestimate the magnitudes of extreme precipitation events relative to gauge-based measurements (Prat & Nelson, 2020). However, IMERG is particularly good at estimating events with short return-periods like the 2-year events examined here (Fang et al., 2019). Using the same dataset to define and detect the extreme events also mitigates the underestimation since the absolute amplitude of the event is not relevant.

MJO phases are determined using the Wheeler–Hendon (2004) index. Only days when the MJO amplitude is greater than one standard deviation are used. Velocity potential anomalies at 200 hPa from CFSR and CFSv2 analyses (Saha et al., 2010b, 2010a, 2011, 2014) are also plotted by MJO phase to illustrate the broader MJO circulation.

3 Defining Extreme Events

Following Bosma et al. (2020), extreme rainfall events are defined herein as 2-year events. The 2-year event threshold is calculated by determining the annual maximum at each gridpoint for each year 2001–2019 (omitting 2000 and 2020, which only had partial data). For each gridpoint, the median of these 19 annual maxima is the 2-year precipitation intensity. Daily rainfall events are examined here, but similar results were obtained for 5-day events (not shown). Since a 2-year event occurs on average once every 730 days, it represents approximately the wettest 0.14% of days (including those without rain), which is much higher than other typical definitions for extreme events like the 75th–95th percentiles.

A 2-year event is advantageous because it is extreme enough to produce societal impacts (Leopold, 1968). However, it is statistically stable since its calculation does not depend on any parameterized extreme value analysis. It is also more useful from a communication standpoint than concepts like a 10- or 100-year flood, which can be confusing to users who are more likely to have a frame of reference for a 2-year event.

Figure **1** compares the mean daily rainfall (top) with the threshold for a 2-year event (bottom). Not surprisingly, both the fields have similar patterns. Areas with heavier mean precipitation are also prone to heavier extreme events. In general, the 2-year event intensity is about 20 times larger than the mean daily rainfall. The 2-year event intensity in desert regions can be as low as 10–20 mm day^{-1}. However, the rarity of precipitation in these areas means that even these small amounts can have societal impacts (Hoell et al., 2018; Nazemosadat & Shahgholian, 2017)

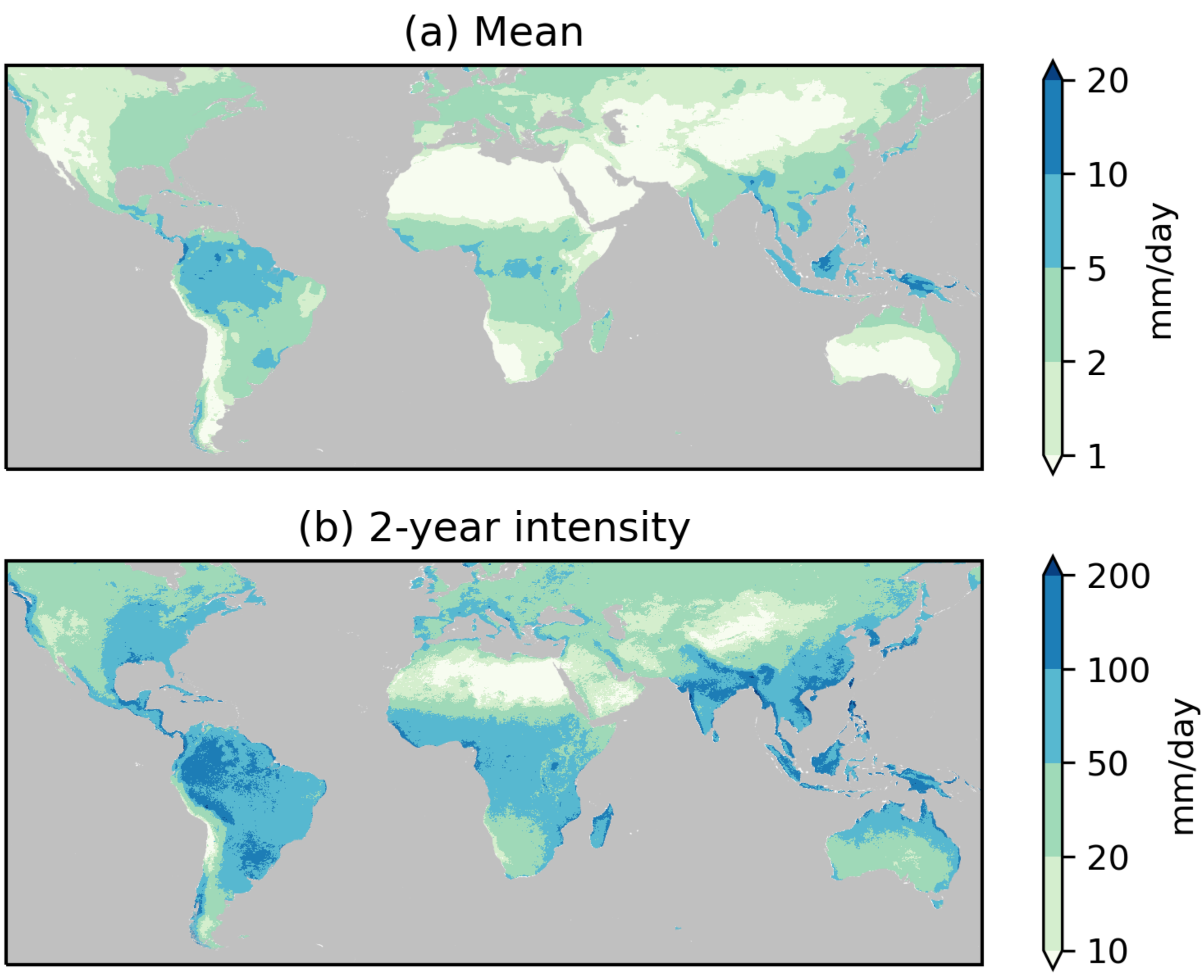

Figure 1. (a) Mean daily rainfall and (b) 2-year event intensity threshold.

Extreme rainfall events also have a strong seasonality (Fig. **2**), which also follows the annual cycle of mean precipitation (not shown). In most regions, these 2-year events can only occur during one or two seasons. Over the Sahel and East Asia, for example, they happen almost exclusively during JJA. On average, these events happen about 0.5 times per year, as may be expected for a 2-year event. However, they can happen >3 times per season for some locations and seasons with particularly strong seasonality.

Statistical significance is evaluated using the cumulative distribution function for a binomial distribution. A point is considered significant (green pixels in Figs. **3**–**6**) if there is less than a 90% chance that the observed number of events would occur during the total number of days in a particular phase given the climatological probability (Fig. **2**).

For example, the MJO spent 268 days in phases 2-3 during DJF (Fig. **3**a). If the climatological frequency were one in two years, then a pixel would be significantly above climatology (green) if it had at least 2 events in the 268 days or about 0.75 events per 100 days. The MJO index spends more days in some phases than others, so the counts per phase are normalized to the number of events per 100 days. Brown pixels are those for which the climatological probability is nonzero but no events were observed for that phase. White pixels are areas where either the number of events is not significantly different from climatology or no events occur during that season regardless of MJO (zero climatology).

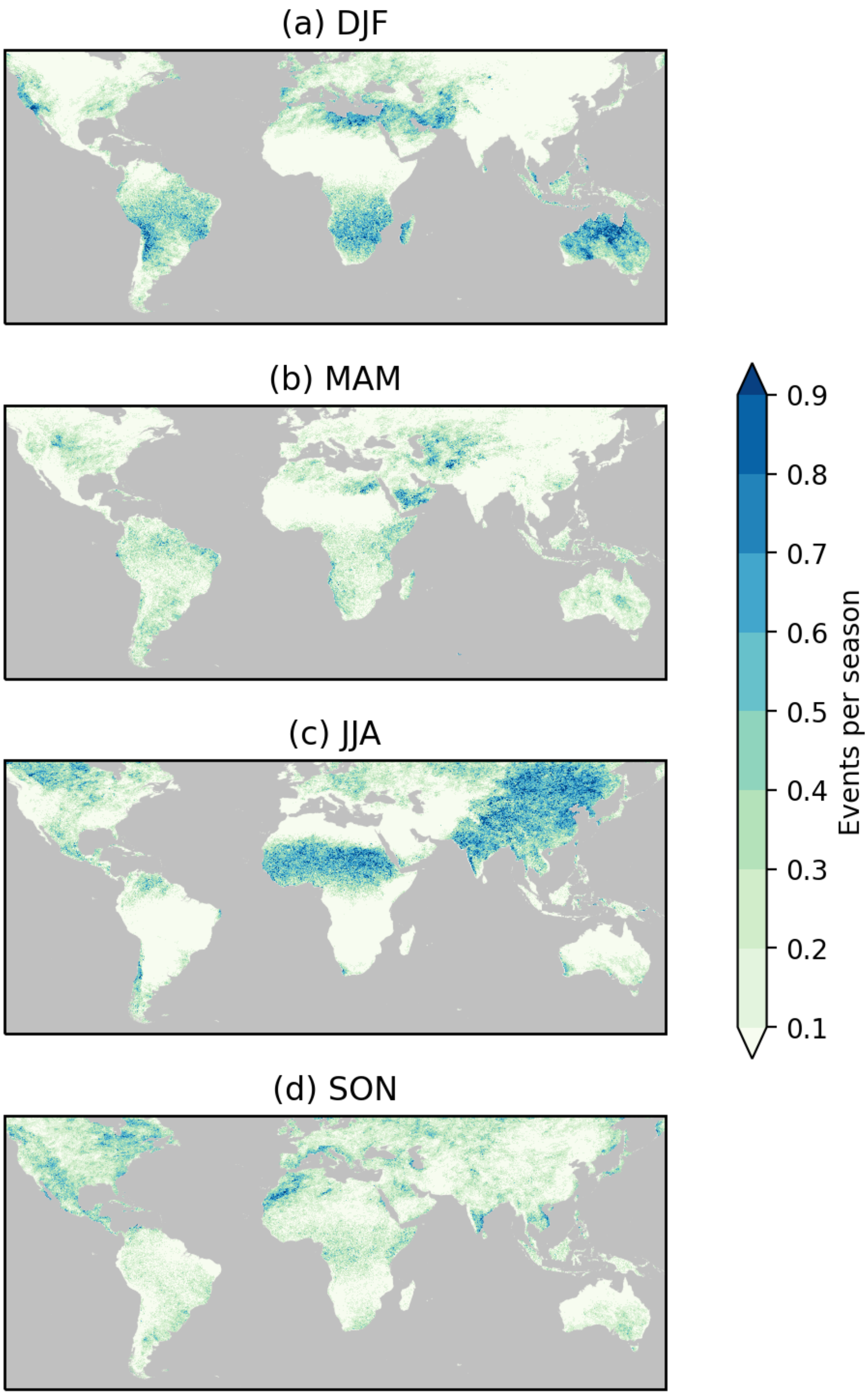

Figure 2. Number of 2-year events by season: (a) DJF, (b) MAM, (c) JJA, and (d) SON.

4 MJO and 2-year Events

Figure **3** illustrates the MJO's impacts on 2-year rainfall events for DJF. It shows the number of events that occur at each IMERG grid point by MJO phase. Extreme rainfall events are rare by definition, and the IMERG data have 0.1° horizontal resolution. As a result, the maps of 2-year events by MJO phase are noisy with areas of significant increases (green) interspersed with those of no significant change (white) or even no events at all (brown).

Even amongst that noise, patterns are apparent in Fig. **3**. In phases 2-3 (Fig. **3**a), for example, 2-year events tend to be more frequent (green) over eastern Brazil and East Africa. Zooming in on the Maritime Continent (Fig. S1a), also shows enhanced extreme events over the Malay Peninsula, southern Sumatra, and western Borneo. During phases 4-5 (Fig. **3**b), the largest enhancements are near the central U.S., northern Argentina (Fig. S2b), and northern Australia (Fig. S1b). These enhancements shift to the Andes and northeastern Australia during phases 6-7 (Fig. **3**c). Phases 8-1 also bring increased events to the U.S. West Coast, eastern Brazil, and Southwest Africa (Fig. **3**d).

In addition to the tropical signals, phases 6-7 demonstrate a strong subtropical enhancement over Egypt, northern Saudi Arabia, and Iraq (Fig. S3a). The increased frequency of 2-year events becomes more widespread across the region in phases 8-1 (Fig. S3d) as the convective phase of the MJO traverses Africa. The threshold for a 2-year event is much lower in these arid regions (Fig. **1**b), which could make these events easier to produce than in wetter regions. Satellite-based precipitation estimates are also particularly uncertain over these arid regions (Fang et al., 2019; Prat & Nelson, 2020). However, neither of these uncertainties could explain the coherent evolution of these events with MJO phase, which are consistent with previous studies of the region (Barlow et al., 2005; Hoell et al., 2018; Mansouri et al., 2021; Nazemosadat et al., 2021; Nazemosadat & Shahgholian, 2017).

The overall results for DJF in Fig. **3** broadly align with Jones et al. (2004, their Fig. 6) for November–May. The higher spatial resolution of the IMERG data allows for a much more detailed picture of the variability over the Maritime Continent (Fig. S1). While Jones et al. observed the increases in extreme events over Southwest Asia during phases 6-7 and 8-1, they lacked the signals over northern Africa (Fig. S3). They also found a weaker signal over Australia that was confined to phases 4-5 (c.f. Fig. S1). Despite these differences, the overall agreement lends confidence in the results presented here.

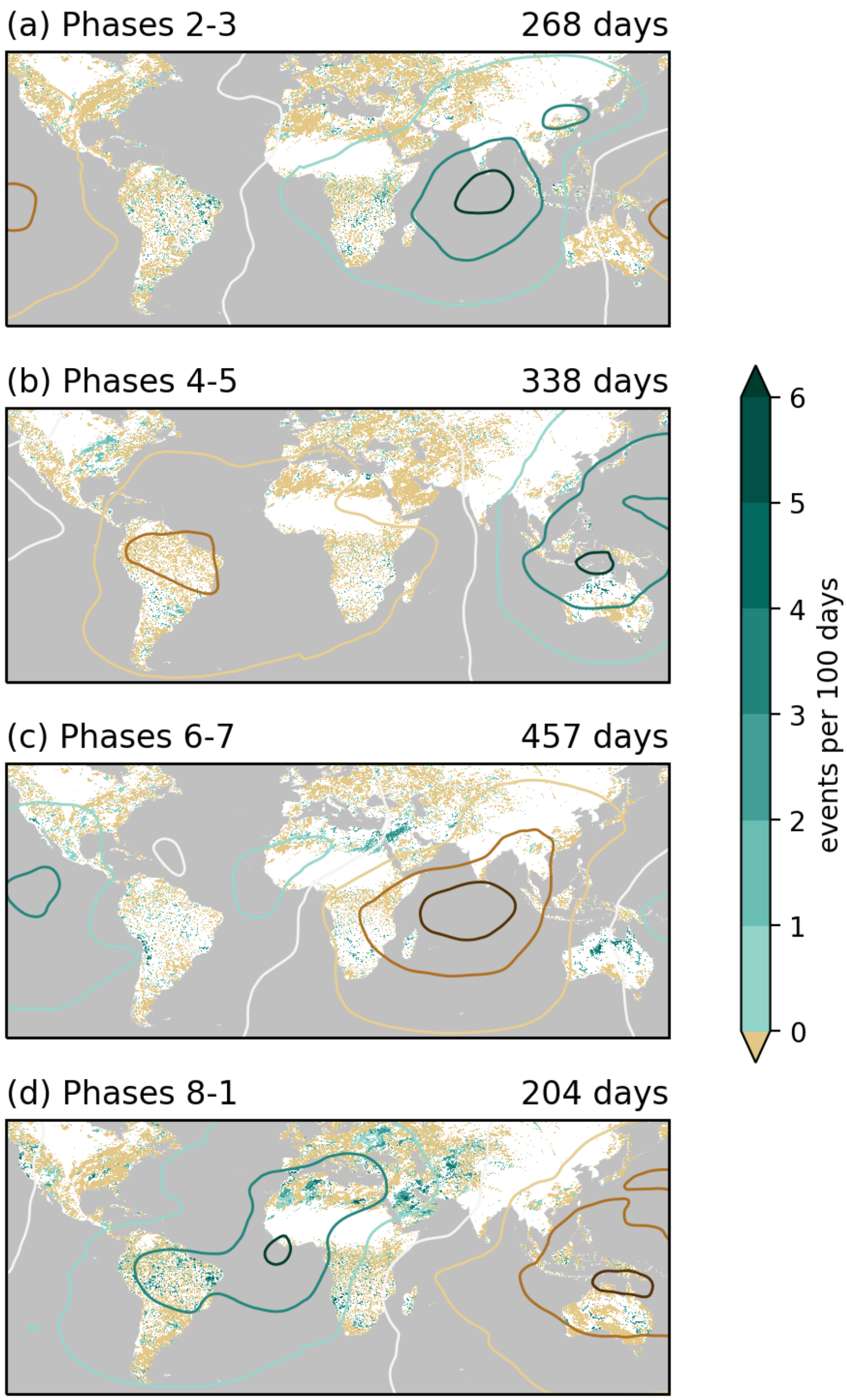

Figure 3. Normalized number of events for DJF in MJO phases (a) 2-3, (b) 4-5, (c) 6-7, and (d) 8-1). White areas are not significantly greater than normal, brown areas have zero events during those phases, and green areas have significantly more events than normal. Contours illustrate the 200-hPa velocity potential anomalies contoured every 2×10^6 m^2 s^{-1} with negative (divergent) values in green and positive (convergent) values in brown.

The occurrence of 2-year events is strongly modulated by the annual cycle (Fig. **2**), and so is the MJO's effect on them. Figure **4** repeats the analysis for MAM when most regions experience fewer extreme precipitation events (Fig. **2**b). North Africa and Southwest Asia experience a similar modulation by the MJO between DJF and MAM with an enhancement in phases 6-7 and 8-1 (Fig. **4**c,d). East Africa is also generally similar between these seasons with the largest enhancement in phases 2-3 and the greatest suppression in phases 6-7.

Australia, on the other hand, has a much less organized pattern during MAM, in part because these events are less common during those months (Fig. **2**b). Australia experiences 2-year events over scattered regions during all the MJO phases with the notable exception of phases 8-1 when they are rare. The clearest signals over South America during MAM are an enhancement over southern Argentina in phases 4-5 (Fig. **4**b) and central Chile in phases 8-1 (Fig. **4**d).

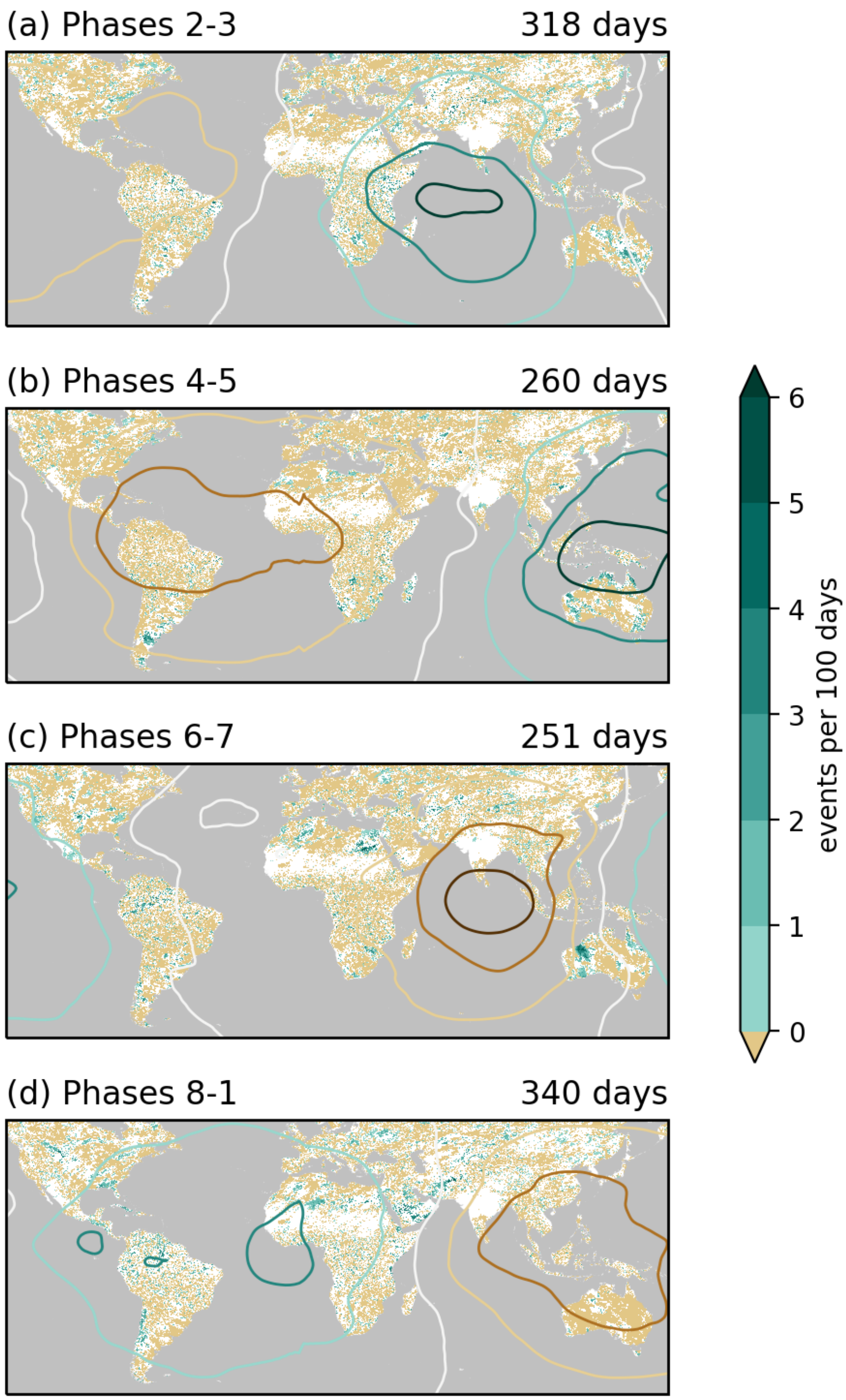

Figure 4. As in Fig. **3** but for MAM.

During JJA, 2-year events are primarily concentrated near the Sahel and East Asia (Fig. **2**c). The Sahel experiences more 2-year events during phases 2-3 (Fig. **5**a, S4a) when the MJO's primary convection is over the Indian Ocean. However, the signal is relatively weak with many areas indistinguishable from their climatological probabilities. Extreme rainfall events are rare over the Sahel during phases 4-5 (Fig. S4b). They are also generally suppressed during phases 6-7 but near-normal during phases 8-1 (Figs. S4c,d).

The MJO's modulation of extreme rainfall is relatively disorganized over East Asia during JJA (Fig. **5**, S5). Their frequency is near-normal during phases 8-1 and 2-3 (Figs. S5d,a). They are suppressed over most of the region during phases 4-5 (Fig. S5b), but several regions have enhanced events including southern India, Southeast Asia, northern China, and the coast of the Yellow Sea. Phases 6-7 are similarly mixed with the enhanced regions shifted northwestward to northern India, northwestern China, South Korea, and northern Japan.

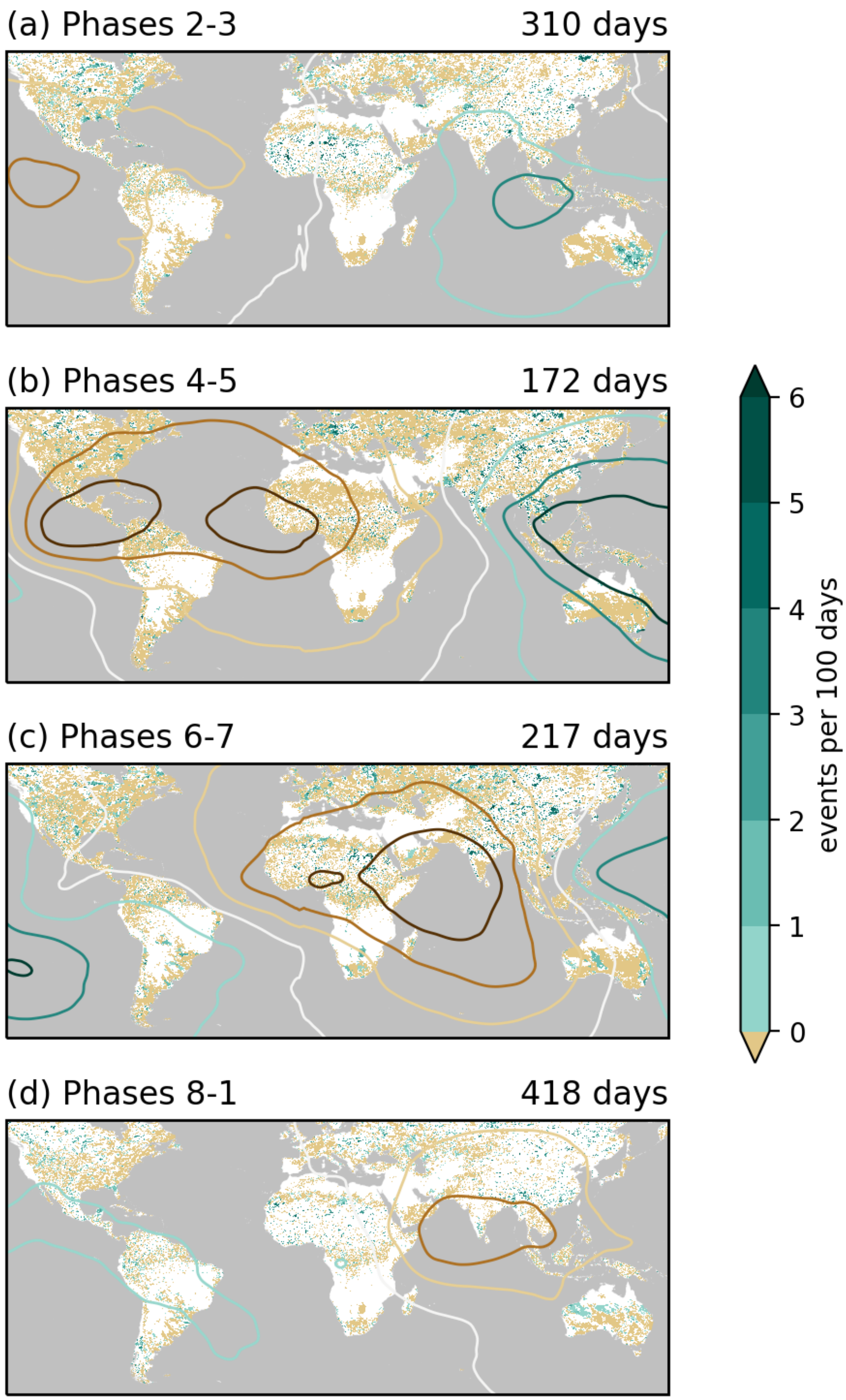

204

205 **Figure 5.** As in Fig. **3** but for JJA.

The global frequency of 2-year events decreases again during SON (Fig. **2**d). The most active regions for these events during SON are North America, northwestern Africa, southern Europe, southern India, and Southeast Asia. The events over the southeastern U.S. are significantly more frequent during phases 2-3 (Figs. **6**a, S6a) and rare during phases 6-7 (Figs. **6**c, S6c). Those patterns align well with the MJO's modulation of Atlantic tropical cyclone activity (Klotzbach, 2010; Kossin et al., 2010), which is the dominant driver of extreme precipitation for that region and season (Kunkel et al., 2010; Prat & Nelson, 2013b, 2013a, 2016).

The MJO relationship is weaker over northwestern Africa and southern Europe with enhanced 2-year events during phases 2-3 and again in phases 6-7 (Figs. **6**a,c). However, they are broadly suppressed in those regions during phases 8-1. Southern India and Southeast Asia predominantly experience these during phases 4-5 in SON (Fig. **6**b).

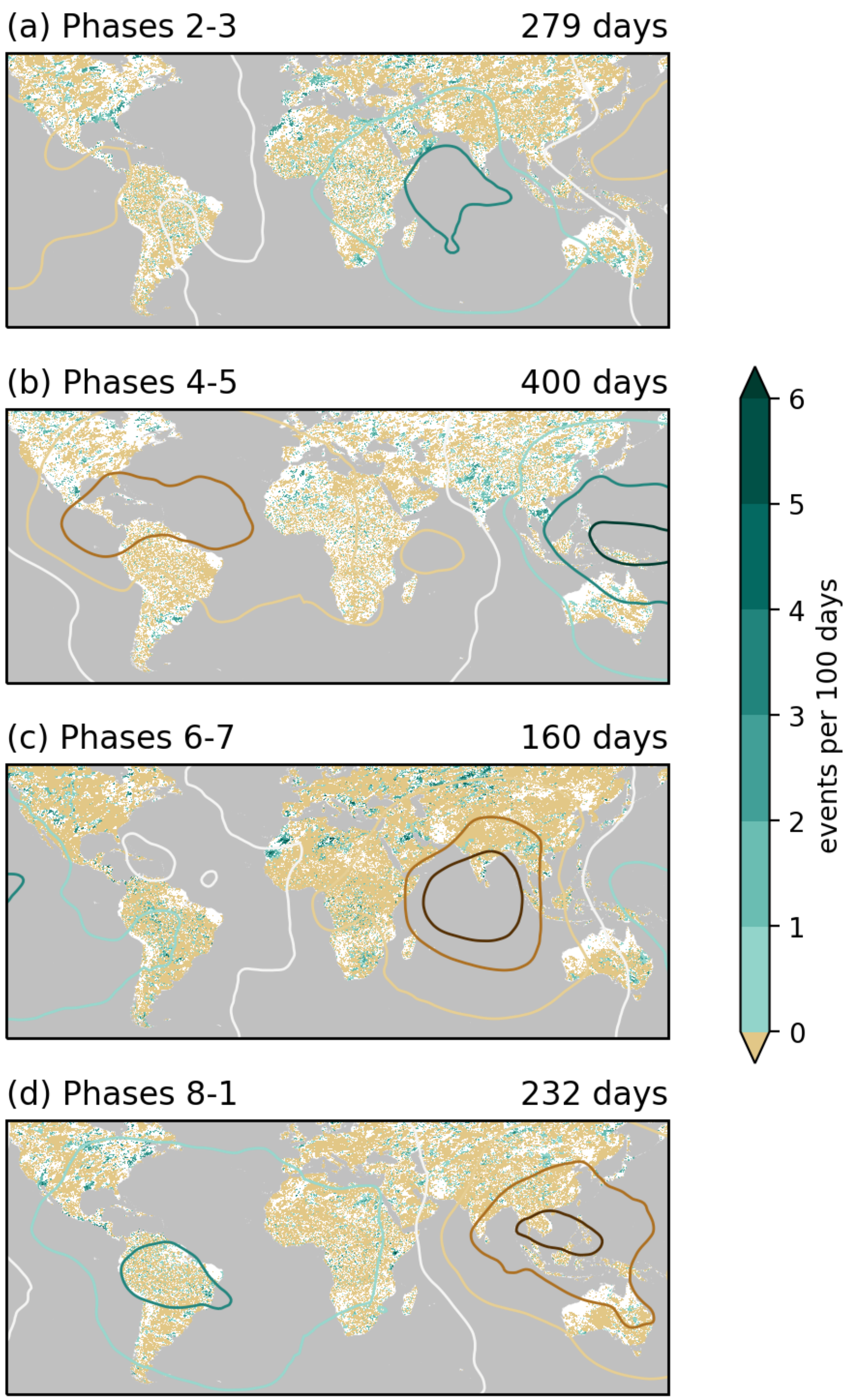

Figure 6. As in Fig. **3** but for SON.

5 Conclusions

This study leverages the unprecedently high spatial resolution and global coverage of the NASA IMERG precipitation data to examine the MJO's impacts on extreme rainfall around the globe. Most studies of the MJO and precipitation extremes have focused on individual regions. Jones et al. (2004) examined the global impacts of the MJO during November–May. The current study extends those results in several ways: examining other seasons, using higher spatial resolution data, focusing on land areas, and using a higher definition of extreme events (2-year events).

While extreme precipitation events tend to follow the MJO's convective phase, they also illustrate significant teleconnections. Both North and South America experience strong seasonally dependent teleconnections. For example, the MJO's modulation of Atlantic tropical cyclone activity leads to variations in extreme rainfall over the Southeast during SON. Another important teleconnection occurs over northern Africa and Southwest Asia during DJF. The synoptic–dynamical underpinnings of these teleconnections need to be explored in greater detail.

These global results point to the need for continued research on the MJO's effects on extreme precipitation. For example, it is not clear why the well-known relationship between the MJO and atmospheric rivers does not show up in stronger modulations of extreme events for the North American West Coast during DJF. Examining other tropical modes like convectively couple equatorial waves (Kiladis et al., 2009) would also be valuable, as their subseasonal modulation of extreme events can overshadow those of the MJO in some regions (Baranowski et al., 2020). The results should also be compared with other global precipitation datasets, although the consistency with the GPCP results from Jones et al. (2004) provides confidence in these results.

Jones et al. (2004) demonstrated the ability of a global circulation model with fixed SSTs to replicate many of these relationships. It would be valuable to examine how that fidelity has improved and how it varies between modern subseasonal models. The results could be leveraged to develop subseasonal forecasts of extreme event probability, which could prove invaluable to farmers and water resource managers.

Acknowledgments

This project was supported by NASA grant NNX16AE33G, NOAA grant NA18OAR4310297, and by NOAA through the Cooperative Institute for Satellite Earth System Studies under Cooperative Agreement NA19NES4320002.

Data Availability Statement

All data used in this manuscript are publicly available. The NASA IMERG data may be obtained from https://doi.org/10.5067/GPM/IMERGDF/DAY/06. The MJO index was obtained from http://www.bom.gov.au/climate/mjo/. CFSv2 data were obtained from https://rda.ucar.edu/datasets/ds094.0/ and the CFSR from https://rda.ucar.edu/datasets/ds093.0/.

References

Baggett, C. F., Barnes, E. A., Maloney, E. D., & Mundhenk, B. D. (2017). Advancing atmospheric river forecasts into subseasonal-to-seasonal time scales. *Geophysical Research Letters*, *44*(14), 7528–7536. https://doi.org/10.1002/2017GL074434

Baranowski, D. B., Flatau, M. K., Flatau, P. J., Karnawati, D., Barabasz, K., Labuz, M., et al. (2020). Social-media and newspaper reports reveal large-scale meteorological drivers of floods on Sumatra. *Nature Communications*, *11*(1), 2503. https://doi.org/10.1038/s41467-020-16171-2

Barlow, M., Wheeler, M., Lyon, B., & Cullen, H. (2005). Modulation of Daily Precipitation over Southwest Asia by the Madden–Julian Oscillation. *Monthly Weather Review*, *133*(12), 3579–3594. https://doi.org/10.1175/MWR3026.1

Bosma, C. D., Wright, D. B., Nguyen, P., Kossin, J. P., Herndon, D. C., & Shepherd, J. M. (2020). An Intuitive Metric to Quantify and Communicate Tropical Cyclone Rainfall Hazard. *Bulletin of the American Meteorological Society*, *101*(2), E206–E220. https://doi.org/10.1175/BAMS-D-19-0075.1

Carvalho, L. M. V., Jones, C., & Liebmann, B. (2004). The South Atlantic Convergence Zone: Intensity, Form, Persistence, and Relationships with Intraseasonal to Interannual Activity and Extreme Rainfall. *JOURNAL OF CLIMATE*, *17*, 21.

Fang, J., Yang, W., Luan, Y., Du, J., Lin, A., & Zhao, L. (2019). Evaluation of the TRMM 3B42 and GPM IMERG products for extreme precipitation analysis over China. *Atmospheric Research*, *223*, 24–38. https://doi.org/10.1016/j.atmosres.2019.03.001

Grimm, A. M. (2019). Madden–Julian Oscillation impacts on South American summer monsoon season: precipitation anomalies, extreme events, teleconnections, and role in the MJO cycle. *Climate Dynamics*, *53*(1–2), 907–932. https://doi.org/10.1007/s00382-019-04622-6

Hirata, F. E., & Grimm, A. M. (2016). The role of synoptic and intraseasonal anomalies in the life cycle of summer rainfall extremes over South America. *Climate Dynamics*, *46*(9–10), 3041–3055. https://doi.org/10.1007/s00382-015-2751-6

Hoell, A., Cannon, F., & Barlow, M. (2018). Middle East and Southwest Asia Daily Precipitation Characteristics Associated with the Madden–Julian Oscillation during Boreal Winter. *Journal of Climate*, *31*(21), 8843–8860. https://doi.org/10.1175/JCLI-D-18-0059.1

Huffman, G. J., Bolvin, D. T., Braithwaite, D., Hsu, K., Joyce, R., Xie, P., & Yoo, S.-H. (2015). NASA global precipitation measurement (GPM) integrated multi-satellite retrievals for GPM (IMERG). *Algorithm Theoretical Basis Document, Version*, *4*, 30.

Huffman, G. J., Stocker, E. F., Bolvin, D. T., Nelkin, E. J., & Tan, J. (2019). GPM IMERG Final Precipitation L3 1 day 0.1 degree x 0.1 degree V06 [Data set]. NASA Goddard Earth Sciences Data and Information Services Center. https://doi.org/10.5067/GPM/IMERGDF/DAY/06

Jones, C., & Carvalho, L. M. V. (2012). Spatial–Intensity Variations in Extreme Precipitation in the Contiguous United States and the Madden–Julian Oscillation. *Journal of Climate*, *25*(14), 4898–4913. https://doi.org/10.1175/JCLI-D-11-00278.1

Jones, C., Waliser, D. E., Lau, K. M., & Stern, W. (2004). Global Occurrences of Extreme Precipitation and the Madden–Julian Oscillation: Observations and Predictability. *Journal of Climate*, *17*(23), 4575–4589. https://doi.org/10.1175/3238.1

Kiladis, G. N., Wheeler, M. C., Haertel, P. T., Straub, K. H., & Roundy, P. E. (2009). Convectively coupled equatorial waves, *47*, RG2003, doi:10.1029/2008RG000266.

Kim, H.-M., Webster, P. J., Toma, V. E., & Kim, D. (2014). Predictability and Prediction Skill of the MJO in Two Operational Forecasting Systems. *Journal of Climate*, *27*(14), 5364–5378. https://doi.org/10.1175/JCLI-D-13-00480.1

Klotzbach, P. J. (2010). On the Madden–Julian oscillation–Atlantic hurricane relationship. *Journal of Climate*, *23*(2), 282–293.

Kossin, J. P., Camargo, S. J., & Sitkowski, M. (2010). Climate modulation of North Atlantic hurricane tracks. *Journal of Climate*, *23*(11), 3057–3076.

Kunkel, K. E., Easterling, D. R., Kristovich, D. A. R., Gleason, B., Stoecker, L., & Smith, R. (2010). Recent increases in U.S. heavy precipitation associated with tropical cyclones. *Geophysical Research Letters*, *37*(24). https://doi.org/10.1029/2010GL045164

Leopold, L. B. (1968). *Hydrology for urban land planning - A guidebook on the hydrologic effects of urban land use* (USGS Numbered Series No. 554). *Hydrology for urban land planning - A guidebook on the hydrologic effects of urban land use* (Vol. 554, p. 26). Reston, VA: U.S. Geological Survey. https://doi.org/10.3133/cir554

Mansouri, S., Masnadi-Shirazi, M. A., Golbahar-Haghighi, S., & Nazemosadat, M. J. (2021). An Analogy toward the Real-Time Multivariate MJO Index to Improve the Estimation of the Impacts of the MJO on the Precipitation Variability over Iran in the Boreal Cold Months. *Asia-Pacific Journal of Atmospheric Sciences*, *57*(2), 207–222. https://doi.org/10.1007/s13143-020-00188-0

Mo, K. C. (2000). The association between intraseasonal oscillations and tropical storms in the Atlantic basin. *Monthly Weather Review*, *128*(12), 4097–4107.

Mundhenk, B. D., Barnes, E. A., Maloney, E. D., & Baggett, C. F. (2018). Skillful empirical subseasonal prediction of landfalling atmospheric river activity using the Madden–Julian oscillation and quasi-biennial oscillation. *Npj Climate and Atmospheric Science*, *1*(1), 7. https://doi.org/10.1038/s41612-017-0008-2

Nazemosadat, M. J., & Shahgholian, K. (2017). Heavy precipitation in the southwest of Iran: association with the Madden–Julian Oscillation and synoptic scale analysis. *Climate Dynamics*, *49*(9), 3091–3109. https://doi.org/10.1007/s00382-016-3496-6

Nazemosadat, M. J., Shahgholian, K., Ghaedamini, H., & Nazemosadat, E. (2021). Introducing new climate indices for identifying wet/dry spells within an Madden-Julian Oscillation phase. *International Journal of Climatology*, *41*(S1). https://doi.org/10.1002/joc.6799

Pohl, B., & Camberlin, P. (2006). Influence of the Madden–Julian Oscillation on East African rainfall: II. March–May season extremes and interannual variability. *Quarterly Journal of the Royal Meteorological Society*, *132*(621), 2541–2558. https://doi.org/10.1256/qj.05.223

Prat, O. P., & Nelson, B. R. (2013a). Mapping the world's tropical cyclone rainfall contribution over land using the TRMM Multi-satellite Precipitation Analysis. *Water Resources Research*, *49*(11), 7236–7254. https://doi.org/10.1002/wrcr.20527

Prat, O. P., & Nelson, B. R. (2013b). Precipitation Contribution of Tropical Cyclones in the Southeastern United States from 1998 to 2009 Using TRMM Satellite Data. *Journal of Climate*, *26*(3), 1047–1062. https://doi.org/10.1175/JCLI-D-11-00736.1

Prat, O. P., & Nelson, B. R. (2016). On the Link between Tropical Cyclones and Daily Rainfall Extremes Derived from Global Satellite Observations. *Journal of Climate*, *29*(17), 6127–6135. https://doi.org/10.1175/JCLI-D-16-0289.1

Prat, O. P., & Nelson, B. R. (2020). Satellite Precipitation Measurement and Extreme Rainfall. In V. Levizzani, C. Kidd, D. B. Kirschbaum, C. D. Kummerow, K. Nakamura, & F. J. Turk (Eds.), *Satellite Precipitation Measurement: Volume 2* (pp. 761–790). Cham: Springer International Publishing. https://doi.org/10.1007/978-3-030-35798-6_16

Ralph, F. M., Neiman, P. J., Kiladis, G. N., Weickmann, K., & Reynolds, D. W. (2011). A multiscale observational case study of a Pacific atmospheric river exhibiting tropical–extratropical connections and a mesoscale frontal wave. *Monthly Weather Review*, *139*(4), 1169–1189. https://doi.org/10.1175/2010MWR3596.1

Saha, S., Moorthi, S., Pan, H.-L., Wu, X., Wang, J., Nadiga, S., et al. (2010a). NCEP Climate Forecast System Reanalysis (CFSR) 6-hourly Products, January 1979 to December 2010 [WMO GRIB2]. UCAR/NCAR - Research Data Archive. https://doi.org/10.5065/D69K487J

Saha, S., Moorthi, S., Pan, H.-L., Wu, X., Wang, J., Nadiga, S., et al. (2010b). The NCEP Climate Forecast System Reanalysis. *Bulletin of the American Meteorological Society*, *91*(8), 1015–1057. https://doi.org/10.1175/2010BAMS3001.1

Saha, S., Moorthi, S., Wu, X., Wang, J., Nadiga, S., Tripp, P., et al. (2011). NCEP Climate Forecast System Version 2 (CFSv2) 6-hourly Products [WMO GRIB2]. UCAR/NCAR - Research Data Archive. https://doi.org/10.5065/D61C1TXF

Saha, S., Moorthi, S., Wu, X., Wang, J., Nadiga, S., Tripp, P., et al. (2014). The NCEP Climate Forecast System Version 2. *Journal of Climate*, *27*(6), 2185–2208. https://doi.org/10.1175/JCLI-D-12-00823.1

Shimizu, M. H., Ambrizzi, T., & Liebmann, B. (2017). Extreme precipitation events and their relationship with ENSO and MJO phases over northern South America: EXTREME EVENTS IN ENSO AND MJO PHASES OVER NORTHERN SOUTH AMERICA. *International Journal of Climatology*, *37*(6), 2977–2989. https://doi.org/10.1002/joc.4893

Vitart, F., & Molteni, F. (2010). Simulation of the Madden– Julian Oscillation and its teleconnections in the ECMWF forecast system. *Quarterly Journal of the Royal Meteorological Society*, *136*(649), 842–855. https://doi.org/10.1002/qj.623

Wheeler, M. C., & Hendon, H. H. (2004). An all-season real-time multivariate MJO index: Development of an index for monitoring and prediction. *Monthly Weather Review*, *132*(8), 1917–1932.

Xavier, P., Rahmat, R., Cheong, W. K., & Wallace, E. (2014). Influence of Madden-Julian Oscillation on Southeast Asia rainfall extremes: Observations and predictability. *Geophysical Research Letters*, *41*(12), 4406–4412. https://doi.org/10.1002/2014GL060241

Zhang, C. (2005). Madden-Julian oscillation, *43*, RG2003, doi:10.1029/2004RG000158. https://doi.org/10.1029/2004RG000158

Zhang, C. (2013). Madden-Julian Oscillation: Bridging Weather and Climate. *Bulletin of the American Meteorological Society*, 130405130926004. https://doi.org/10.1175/BAMS-D-12-00026.1

Zhang, C., Gottschalck, J., Maloney, E. D., Moncrieff, M. W., Vitart, F., Waliser, D. E., et al. (2013). Cracking the MJO nut. *Geophysical Research Letters*, *40*(6), 1223–1230. https://doi.org/10.1002/grl.50244